Supramolecular tripeptide self-assembly initiated at the surface of coacervates by polyelectrolyte exchange

Miryam Criado-Gonzalez, Deborah Wagner, Muhammad Haseeb Iqbal, Aymeric Ontani, Alain Carvalho, Marc Schmutz, Joseph Schlenoff, Pierre Schaaf, Loïc Jierry, Fouzia Boulmedais

Supramolecular Tripeptide Self-Assembly Initiated at the Surface of Coacervates by Polyelectrolyte Exchange

Miryam Criado-Gonzalez,[a,b] Deborah Wagner,[a] Muhammad Haseeb Iqbal,[a] Aymeric Ontani,[a] Alain Carvalho,[a] Marc Schmutz,[a] Joseph B. Schlenoff,[c] Pierre Schaaf,*[a,b] Loïc Jierry,[a] Fouzia Boulmedais*[a]

a. Université de Strasbourg, CNRS, Institut Charles Sadron (UPR 22), 23 rue du Loess, BP 84047, 67034 Strasbourg Cedex 2 (France).

b. Institut National de la Santé et de la Recherche Médicale, INSERM Unité 1121, "Biomatériaux et Bioingénierie", 1 rue Eugène Boeckel 67000 Strasbourg (France) and 8 rue Sainte Elisabeth 67000 Strasbourg (France).

c. Florida State University, Department of Chemistry and Biochemistry, Tallahassee, 32306 Florida, United States.

***Corresponding authors.** E-mail: fouzia.boulmedais@ics-cnrs.unistra.fr; schaaf@unistra.fr

Tel: +33 03 88 41 41 60

ABSTRACT

Spatial control of supramolecular self-assembly can yield compartmentalized structures, a key feature for the design of artificial cells. Inducing self-assembly *from* and *on* compartments is still a challenge. Polyelectrolyte complex coacervates are simple model droplet systems able to reproduce the basic features of membrane-less organelles, appearing in cells. Here, we demonstrate the supramolecular self-assembly of a phosphorylated tripeptide, Fmoc-FFpY (Fmoc: fluorenyl-methoxycarbonyl; F: phenyl alanine, pY: phosphorylated tyrosine), on the surface of poly(L-glutamic acid)/poly(allylamine hydrochloride) (PGA/PAH) complex coacervate microdroplets. The phosphorylated peptides self-assemble, without dephosphorylation, through ion pairing between the phosphate groups of Fmoc-FFpY and the amine groups of PAH. This process provides spontaneous capsules formed by an amorphous polyelectrolyte complex core surrounded by a structured peptide/PAH shell. Similar fibrillar Fmoc-FFpY self-assembled structures are obtained at the interface between the peptide solution and a PGA/PAH polyelectrolyte multilayer, a complex coacervate in the thin film or "multilayer" format. In contact with the peptide solution, PAH chains diffuse out of the coacervate or multilayer film and complex with Fmoc-FFpY at the solution interface, exchanging any PGA with which they were associated. Self-assembly of Fmoc-FFpY, now concentrated by complexation with PAH, follows quickly.

Keywords: Coacervates, polyelectrolytes, peptides, supramolecular self-assembly, layer-by-layer, multilayers, Fmoc-FF

1. Introduction

Biological cells represent highly evolved complex chemical systems governed by the interplay between a myriad of chemical reactions and localized self-assembly processes. Mitotic spindles initiated at centrosomes, membrane-less organelles [1], are one example of such highly integrated processes [2]. Membrane-less organelles have attracted great attention from the scientific community over the last few years since they appear to result from phase separation processes allowing for a rapid response of the cellular machinery to external stimuli [3]. They are often viewed as liquid-like phase-separated condensates of numerous proteins interacting mainly through intrinsically disordered domains. Polyelectrolyte complex coacervates are simple model droplet systems to address specific features of membrane-less organelles [4, 5]. In the quest to learn about the origins of life and to gain better insight into general concepts underlying cellular mechanisms, one of the goals of science is to create artificial (synthetic) cells [6, 7] possessing essential features of biological ones. In particular, they must contain several compartments for localizing incompatible reactions or initiating local self-assembly [8]. Multicompartment systems have been designed from polymer capsules containing liposomes [9], small polymer vesicles [10-13] or, more recently, complex coacervates containing polymersomes [4, 14]. Inducing self-assembly *from* and *on* compartments is another challenge. To the best of our knowledge, only one such system has been reported so far consisting of polypeptide coacervates, known to partition proteins in solution, which polymerized actin forming long fibers localized around the coacervate droplets [15].

In recent years, our group has concentrated on Fmoc-peptide self-assembly localized at surfaces where non-self-assembling peptides are transformed enzymatically into hydrogelators [16, 17]. We mainly used phosphorylated Fmoc-FFpY (Fmoc: fluorenyl-methoxycarbonyl; F: phenyl

alanine, pY: phosphorylated tyrosine) peptides, which are dephosphorylated by alkaline phosphatase. Recently, we found that Fmoc-FFpY self-assembly can be initiated *without* dephosphorylation by mixing it with polycations, leading to micrometer-long fibers [18]. Fmoc-FFpY/polycation hydrogels were formed by ion pairing between the phosphate groups of Fmoc-FFpY and the amine groups of polycation. Using this strategy, we present here a synthetic system where the peptide self-assembly is initiated from and localized around complex coacervates composed of poly(allylamine hydrochloride) (PAH) as polycation and poly(L-glutamic acid) (PGA) as polyanion. After formation, PGA/PAH coacervates were exposed to Fmoc-FFpY peptides to induce peptide self-assembly leading to core/shell structures combining a polymer core surrounded by a shell composed of PAH and self-assembled peptides (Scheme 1).

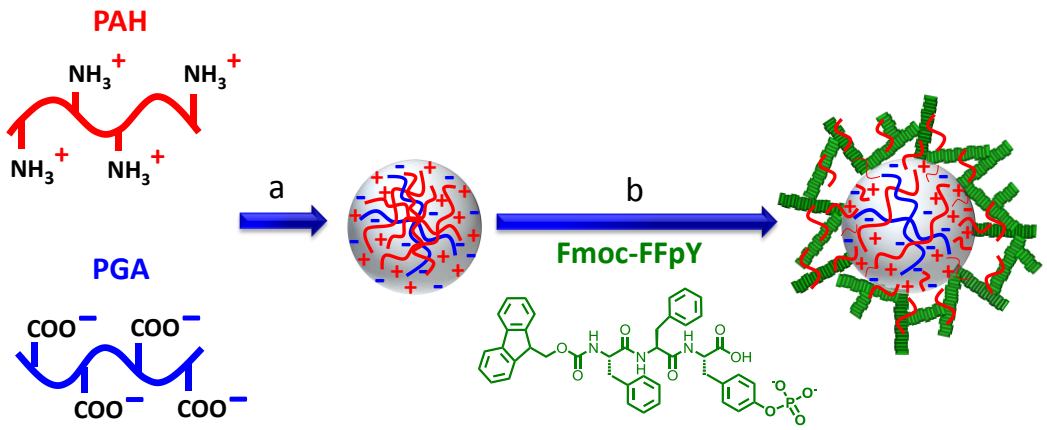

Scheme 1. Representation of two-step strategy: (a) PGA/PAH coacervates obtained by electrostatic interaction between polyelectrolytes followed by (b) exposure to Fmoc-FFpY peptides, which self-assemble at the surface of coacervates via ion pairing between Fmoc-FFpY and PAH leading to (c) a hybrid supramolecular hydrogel undergoing a phase separation over time.

2. Materials and methods

2.1. Materials

Poly(allylamine hydrochloride) (PAH, M_w = 120 000 g mol^{-1}) and branched poly(ethylene imine) (PEI, M_w = 100 000 g mol^{-1}, 30% aqueous solution) were provided by Alfa Aesar. Fmoc-FFpY (99% purity) was purchased by PepMic. Poly-(L-glutamic acid) sodium salt (PGA, M_w = 97 800 g mol^{-1}), Poly(styrene sulfonate) (PSS, M_w = 70 000 g mol^{-1}), Thioflavin T (ThT), N-(3-Dimethylaminopropyl)-N'-ethyl-carbodiimide hydrochloride (EDC) and N-Hydroxy sulfo-succinimide sodium salt (NHS) were provided by Sigma Aldrich. Sodium tetraborate anhydrous (borax) was supplied by Acros Organics and Sodium chloride by VWR. All products were used without further purification.

2.2. Coacervate preparation and Fmoc-FFpY self-assembly

All polyelectrolytes were prepared in 0.15 M NaCl adjusted to pH 9.5 using 1 M NaOH. 100 µL of PAH (105.4 mM in monomer or 9.8 mg mL^{-1}) and 100 µL of PGA (49.4 mM or 8.4 mg mL^{-1}) were mixed simultaneously to obtain PGA/PAH coacervates. For the self-assembly of Fmoc-FFpY around the coacervates, 20 µL of 2 mg mL^{-1} (2.6 mM) Fmoc-FFpY solution, prepared in 25 mM borax buffer at pH 9.5, was put in contact with 200 µL PGA/PAH coacervate suspension.

2.3. Zeta potential

Zeta potential was measured using a Malvern Nanosizer NanoZS instrument equipped with a 4 mW He-Ne laser (λ = 633 nm) at a scattering angle of 173º. PGA/PAH coacervates were obtained by mixing 0.98 mg mL^{-1} PAH and 0.84 mg mL^{-1} PGA solutions in equal volumes of 450 µL. 90 µL of 2 mg mL^{-1} Fmoc-FFpY was added to the coacervate solution. The zeta

potential measurements were performed at 25 ºC by conducting 20 runs using polystyrene cuvettes (SARSTEDT). The electrophoretic mobility was transformed into zeta potential using the Smoluchowski equation and ZetaSizer Software version 7.10. The average and standard deviation of the zeta potential were calculated from three measurements.

2.4. Multilayer film preparation and Fmoc-FFpY self-assembly

All polyelectrolyte solutions were prepared in 0.15 M NaCl adjusted to pH 9.5. Multilayer films were built on 14 mm diameter glass slides (Marienfeld). As the substrates are negatively charged, a precursor layer of PEI (23.3 mM or 1 mg mL^{-1}) was deposited to obtain a positively charged substrate. For this, substrates were immersed in a solution of PEI for 10 min followed by two rinsing steps with 0.15 M NaCl for 5 min. The multilayer film was built up through sequential dipping of the substrate into the PSS (polyanion) and PAH (polycation) solutions for 10 min with two rinsing steps in 0.15 M NaCl for 5 min after each polyelectrolyte deposition. This cycle was repeated 3 times. Then the substrate was alternately immersed in PGA (12.4 mM or 2.1 mg mL^{-1}) (polyanion) and PAH with 5% PAH^{rho} (26.9 mM or 2.5 mg mL^{-1}) solutions for 10 min with three intermediate rinsing steps in 0.15 M NaCl for 5 min after each polymer deposition. This cycle was repeated 23.5 times. The obtained PEI-$(PSS/PAH)_3$-$(PGA/PAH^{rho})_{23}$-PGA films are denoted $(PGA/PAH^{rho})_{23}$-PGA. Subsequently, 2 mg mL^{-1} Fmoc-FFpY solution, prepared in 25 mM borax buffer pH 9.5 containing 0.15 mg mL^{-1} ThT, was brought in contact with the multilayer film for 16 h before observation by CLSM.

2.5. Confocal Laser Scanning Microscopy (CLSM)

Confocal laser scanning microscopy images (CLSM) were captured with a Zeiss LSM 710 microscope using an EC Plan-Neofluar 10x/0.3, Plan-Apochromat 20x/0.8 M27 and EC Plan-Neofluar 40x/0.75 M27 objectives. PAH was prepared with 5% of labelled PAH with rhodamine-B (PAH^{rho}) using a standard protocol (Mertz et al. *Soft Matter* 2007, 3, 1413-1420). The fluorescence of rhodamine was measured with excitation at 561 nm and emission was filtered between 566 and 703 nm. The peptide self-assembly was visualized by adding thioflavin T (0.15 mg mL^{-1}) in the solution of Fmoc-FFpY. The fluorescence of the thioflavin T was measured by excitation with an argon laser with a cut-off dichroic mirror at 488 nm and an emission band-pass filter between 493 and 548 nm. Coacervates were formed by mixing directly over the glass substrate 100 µL of PAH^{rho} (105.4 mM or 9.8 mg ml^{-1} in NaCl 0.15M pH 9.5) with 100 µL of PGA (49.4 mM or 8.4 mg ml^{-1} in NaCl 0.15M pH 9.5). Then, 20 µL of a Fmoc-FFpY solution (2 mg mL^{-1} or 2.6 mM in borax buffer containing 0.15 mg mL^{-1} ThT) were added to the coacervates.

2.6. Circular dichroism (CD)

CD spectra were recorded from190 to 320 nm using a Jasco J-1100 spectropolarimeter with a data pitch of 1 nm on the wavelength. Samples were measured using quartz slides of 1 mm thickness. Samples were placed between the two slides leading to a path length of about 0.1 mm.

2.7. Fourier Transform Infrared spectroscopy (FTIR)

FTIR experiments were performed on a Vertex 70 spectrometer (Bruker, Germany) using a DTGS detector. Spectra were recorded in the Attenuated Total Reflection (ATR) mode using a single reflection diamond ATR for coacervates and using a ZnSe crystal (45° 72 ×

10 × 6 mm^3 trapezoidal, six reflections,) for layer-by-layer films by averaging 128 interferograms between 600 and 4000 cm^{-1} at 2 cm^{-1} resolution, using Blackman-Harris three-term apodization and Bruker OPUS/IR software (version 7.5). All solutions were prepared in D_2O to minimize the water peak in the region of the amide I band. PGA (10 mg mL^{-1}) and PGA/PAH mixture (1:2 PGA/PAH molar ratio at 10 mg mL^{-1}) were prepared in 0.15 M NaCl adjusted to pH 9.5. PEI-$(PGA/PAH)_{23}$-PGA LbL films were built with the same procedure described in section 1.3 in deuterated solutions. The FTIR spectrum of the PGA/PAH LbL film was recorded after rinsing with borax buffer before contact with Fmoc-FFpY solution. FTIR spectra of Fmoc-FFpY self-assembly on PGA/PAH LbL were recorded every 15 min after contact with the peptide solution. To decompose the amide I band, data processing was performed using Bruker OPUS/IR software (version 7.5). Spectra were smoothed using a five point smoothing function, cut between 1600 and 1720 cm^{-1} and then normalized using a "min-max" normalization method. The baseline was then adjusted to calculate the second derivative. The number and the frequencies of the different components, forming the amide I band, were determined by means of the second derivative of the Fourier smoothed spectrum using the minimum positions. The decomposed spectrum was fitted with Gaussian band profiles using Multiple Peak Fit. The quality of the fitting was estimated by the residual RMS provided by the software. The relative contribution of each component of the amide I band was calculated by the ratio of the area of each peak to the area of the total amide I band.

2.8. Fluorescence spectroscopy

All fluorescence spectra were recorded between 300-550 nm using a Fluoromax-4 (Horiba Jobin Yvon - Edison, NJ USA) at an excitation wavelength of 290 nm using a quartz cuvette of 1 mm path length.

2.8. Quartz crystal microbalance with dissipation monitoring (QCM-D)

QCM-D experiments were performed in a QCM-D cell on a Q-Sense E1 apparatus (Q-Sense AB, Gothenburg, Sweden) at 22 °C. The resonance frequencies of a gold coated crystal and the dissipation factors at four frequencies, the fundamental frequency at 5 MHz ($\nu = 1$) and the 3rd, 5th and 7th harmonics ($\nu = 3$, 5 and 7) at 15, 25 and 35 MHz, respectively were monitored. The QCM-D experiments give information on the adsorption process. Polyelectrolyte deposition and rinsing steps were performed by injection of 600 µL of the solution at 600 µl min^{-1}. A precursor layer of PEI (23.3 mM or 1 mg mL^{-1}) was deposited for 10 min followed by a rinsing step with 0.15 M NaCl for 5 min. The multilayer film was built up through alternating deposition of PGA (5.9 mM or 1 mg mL^{-1} in 0.15 M NaCl pH 9.5) and PAH (12.9 mM or 1.2 mg mL^{-1} in 0.15 M NaCl pH 9.5) solutions for 10 min with a rinsing step in 0.15 M NaCl for 5 min after each polyelectrolyte deposition. This cycle was repeated 5.5 times and PEI-$(PGA/PAH)_5$-PGA samples were denoted as $(PGA/PAH)_5$-PGA. Subsequently, a solution of Fmoc-FFpY (2 mg mL^{-1} in 25 mM borax buffer pH 9.5) was brought in contact with the multilayer film for 17 h. In the case of the cross-linked film, after the buildup described previously, $(PGA/PAH)_5$-PGA film was put in contact with a solution of 400 mM EDC with 100 mM NHS for 20 h. Subsequently, 2 mg mL^{-1} Fmoc-FFpY solution, prepared in 25 mM borax buffer pH 9.5, was brought in contact with the multilayer film for 7 h.

2.10. Scanning Electron Microscopy (SEM) and Cryo-SEM

A specialized cryo-holder and a cryo preparation chamber, designed and manufactured by the machine shop facility of the Charles Sadron Institute were employed for SEM observations. $(PGA/PAH)_{23}$-PGA film, deposited on a silicon wafer, was placed on the cryo-holder to be quickly plunged into an ethane slush. As the sample was free standing over the holder, the sample was rapidly frozen during immersion by direct contact with the liquid ethane. Subsequently, the sample was transferred into the Quorum PT 3010 cryo-chamber attached to the microscope. There, the frozen sample was fractured with a razor blade. A slight etching at -90°C was performed to render the fibers more visible. The sample was then transferred in the FEG-cryo SEM (Hitachi SU8010) and observed at 1 kV at -150°C.

3. Results and discussion

3.1 PGA/PAH coacervates characterization

PGA/PAH coacervates were formed by simple mixing of both polyelectrolyte solutions, prepared in 0.15 M NaCl pH 9.5. The doping of PAH solution by 5% PAH^{rho} (PAH labelled with rhodamine B) allowed the analysis of PGA/PAH^{rho} coacervates by confocal laser scanning microscopy (CLSM). Spherical droplets were obtained with an average size of 3.4 ± 0.6 µm (Fig. 1a-b). A cross-section of the fluorescence of an individual coacervate droplet exhibits a curve with a maximum in intensity located at the center, probably due to its spherical shape (Fig. 1c-d).

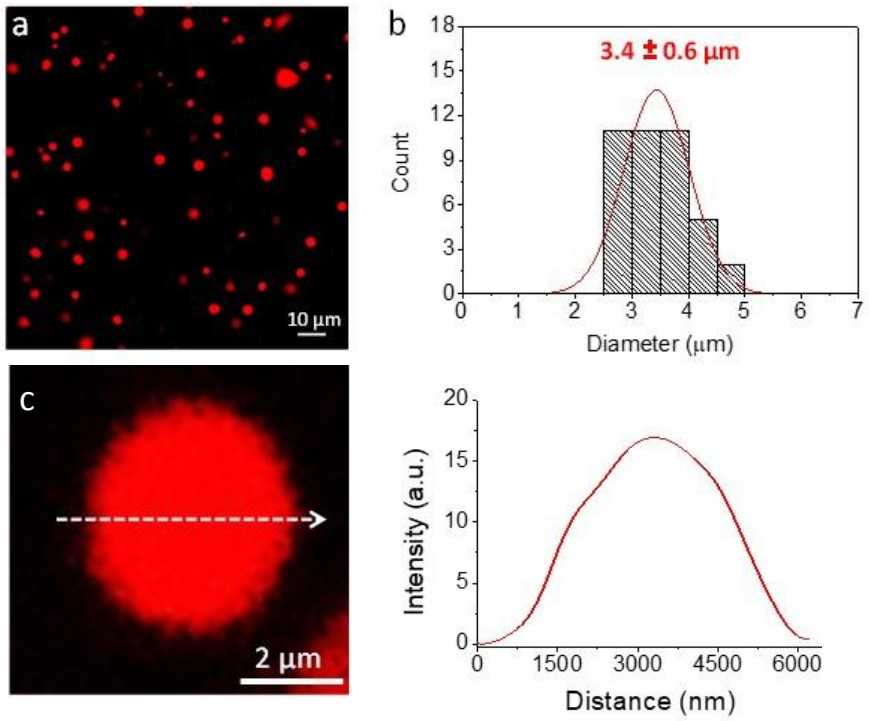

Fig. 1. PGA/PAH^{rho} coacervates, formed with PAH containing 5% PAH^{rho}, (a) CLSM image and (b) histogram of their diameters, obtained from image (a) using ImageJ. The average size, determined by counting 40 coacervates, was 3.4 ± 0.6 µm. (c) Magnification of one coacervate and (d) its fluorescence intensity profile along the white arrow.

3.2 Fmoc-FFpY self-assembly on PGA/PAH coacervates

With a 1.56 molar ratio of charges in PGA/PAH, the coacervates are negatively charged with a zeta potential of -24 ± 2 mV. The addition of negatively charged Fmoc-FFpY peptide should not induce a precipitation of the coacervates. After addition of Fmoc-FFpY solution, the zeta potential reached a value of -21 ± 3 mV. In CLSM experiments, Thioflavin T (ThT), a non-fluorescent probe that emits green fluorescence when incorporated into β-sheets, was mixed with Fmoc-FFpY solution to visualize the peptide self-assembly [19]. When the Fmoc-FFpY solution was added to the PGA/PAH^{rho} coacervate solution, a green fluorescence was immediately observed and localized only around the droplets (Fig. 2a-c).

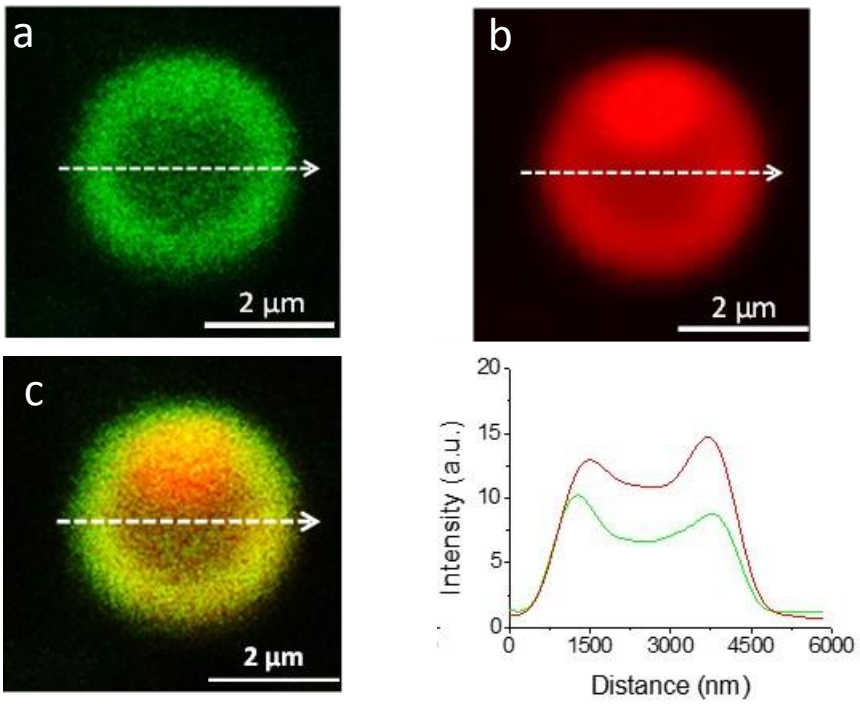

Fig. 2. CLSM images of one Fmoc-FFpY-coacervate droplet, obtained by contact of PGA/PAH^{rho} coacervates with Fmoc-FFpY solution in the presence of ThT, (a) in the green, (b) red and (c) merged channels with (d) the fluorescence intensity profile along the white arrow.

A more intense green, related to the peptide self-assembly, is visible on the periphery of the spherical droplet. Similarly, in comparison to the center of the coacervates, a higher red intensity due to PAH^{rho} is observed on the periphery superimposed on the green image (Fig. 2b-c). The cross-section of the fluorescence of the droplet shows a curve with two maxima in intensity located at the edge (Fig. 2d). To better observe the peptide self-assembly, the coacervates were first adhered for a few minutes to a glass substrate to immobilize them before contact with Fmoc-FFpY solution (Fig. 3a and S1).

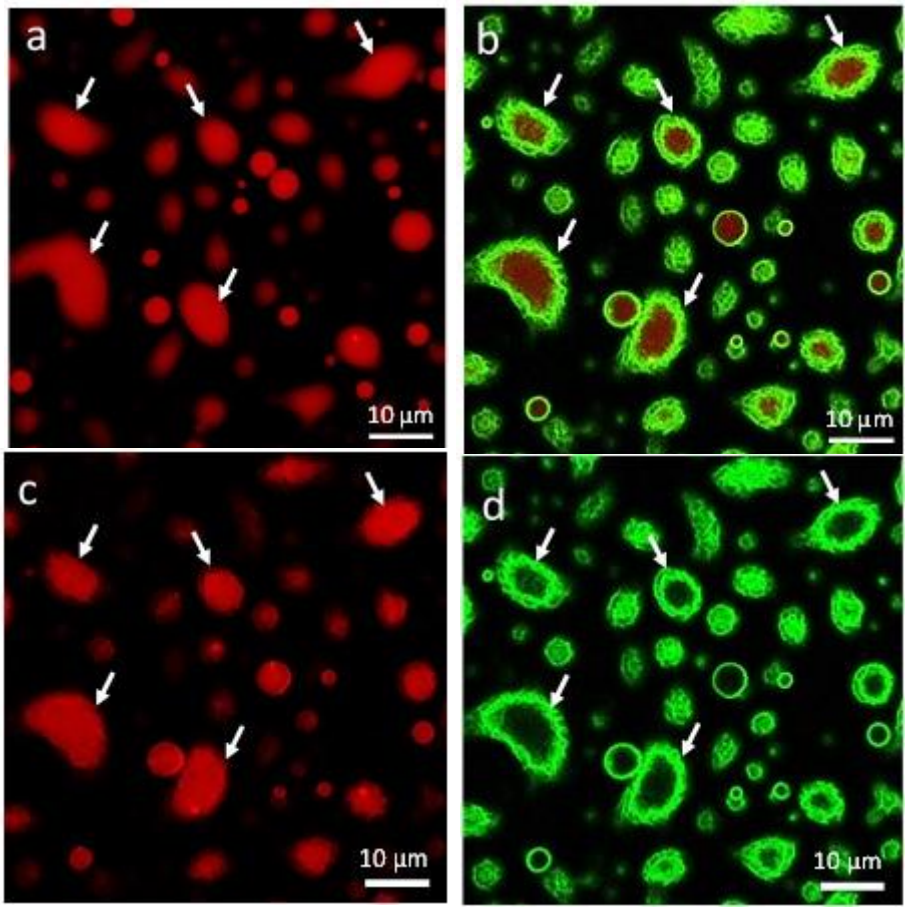

Fig. 3. CLSM images of PGA/PAH^{rho} coacervates adhered to a glass substrate, observed in merged channel, (a) before and (b) a few seconds after Fmoc-FFpY self-assembly, in the presence of ThT, and in (c) green and (d) red channels in the latter case. White arrows show deformed coacervate droplets due to their adhesion to the surface.

In this case, droplets were larger than in solution and deformed losing their round shape (Fig. 3a, white arrows). When Fmoc-FFpY solution was added, an entanglement of fibers was formed around the coacervates leading to a shell (Fig. 3b-d). This phenomenon is clearly observed by superposing the fluorescent images of the different channels (Fig. 3b-c). Fmoc-FFpY self-assembled on the coacervates, termed Fmoc-FFpY-coacervates, have a core-shell structure formed by a polymer core surrounded by a self-assembled PAH/Fmoc-FFpY shell [18]. The

thickness of the shell depends on the initial size of the coacervate droplets. To confirm the peptide self-assembly, PGA/PAH coacervates and Fmoc-FFpY-coacervates were further studied by circular dichroism (CD), and fluorescence spectroscopy. CD shows the conformation of coacervates before and after contact with Fmoc-FFpY solution (Fig. 4a, HT spectra Fig. S2b).

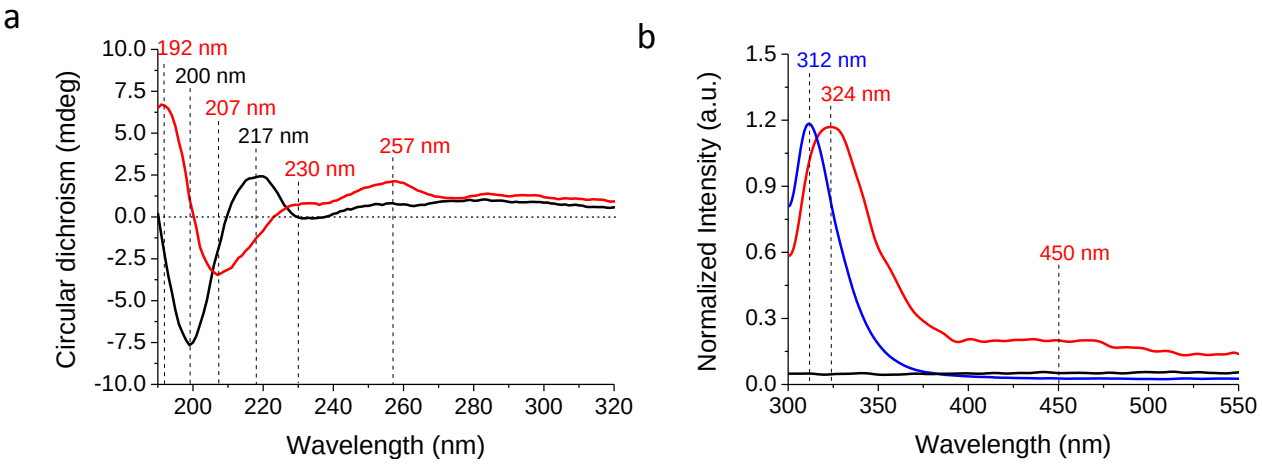

Fig. 4. (a) CD and (b) fluorescence spectra, normalized to the peak at 312 nm, of Fmoc-FFpY (blue curve) and PGA/PAH coacervates before (black curve) and after (red curve) contact with Fmoc-FFpY.

As with PGA in solution, the CD spectrum of the PGA/PAH coacervates shows a strong negative peak at 200 nm and a positive band at 217 nm, which are characteristic of a random coil conformation [20]. After contact with Fmoc-FFpY solution, Fmoc-FFpY-coacervates show a positive peak located at 192 nm together with a negative band centered at 207 nm, attributed to β-sheets [21]. In comparison, the CD spectrum of Fmoc-FFpY solution, at the same concentration added to the coacervates, showed a noisy signal because of the insufficient quantity of material (Fig. S2c). Fmoc-FFpY peptides self-assembled in β-sheets structures. Moreover, Fmoc-FFpY-coacervates spectra have two maxima at 230 and 257 nm which is the signature of stacking interactions of the aromatic units of Fmoc-FFpY [22]. Fluorescence

spectroscopy was used to check the excimer formation of Fmoc moieties, another signature of the peptide self-assembly. The Fmoc-FFpY peptide (blue curve) shows a band at 312 nm attributed to fluorenyl moieties in the non-self-assembled state (Fig.4b) [23, 24]. When the peptide is brought in contact with PGA/PAH coacervates, a shift up to 324 nm is observed instantaneously, attributed to fluorenyl excimers [18, 23]. The broad band at 450 nm is attributed to J-aggregates formed by multiple aromatic groups, including phenyl and fluorenyl rings, stacked through π-π interactions [23, 24]. Similar results were obtained for a mixture of Fmoc-FFpY and PAH [18]. No fluorescence shift is observed for Fmoc-FFpY/PGA meaning that no interaction takes place between these components (Fig. S3).

3.3 Fmoc-FFpY self-assembly on PGA/PAH Layer-by-Layer film

The origin of the localized peptide self-assembly around the coacervates can be attributed to the ability of PAH chains to diffuse out from the interior of the droplets and to interact with Fmoc-FFpY peptides in solution. This is strongly similar to the mechanism explaining the exponential growth of Layer-by-Layer (LbL) films, which is due to the diffusion of the polyelectrolytes throughout the film during the deposition steps. Not stratified, exponentially growing films are highly hydrated (up to 80–90% of water in volume fraction) [25], as are coacervates, and show a high polyelectrolyte chain mobility in all directions [26]. Known to display exponential growth [27], PGA/PAH multilayer films terminated with PGA were used as a 2D model of PGA/PAH coacervates to gain more insight on the peptide self-assembly mechanism. Two PGA/PAH films with different numbers of bilayers were built depending on the characterization techniques used. $(PGA/PAH)_{23}$-PGA film has a thickness of a few µm which can be observed by Cryo-Scanning Electron Microscopy (Cryo-SEM) and CLSM allowing discrimination of the peptide self-

assembly from the film. The cross-section of the fluorescent PGA/PAH^{rho} film was observed by CLSM before (Fig. S4) and after contact with the Fmoc-FFpY peptide (Fig. 5).

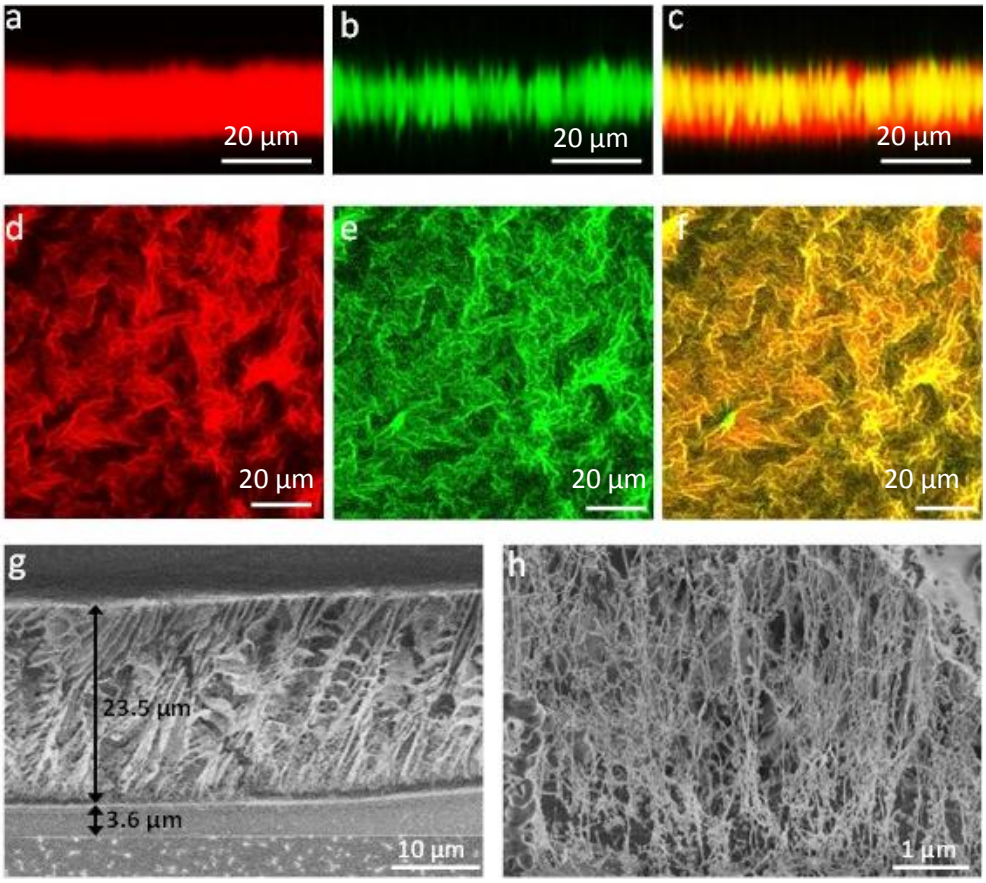

Fig. 5. Cross-section of Fmoc-FFpY self-assembled on top of (PGA/PAH^{rho})$_{23}$-PGA multilayer film observed by (a-f) CLSM in the (a) red, (b) green and (c) merged channels with the respective top views (d, e and f) and (g) Cryo-SEM (large cavities on the upper part may be due to the sublimation of ice crystals) with (h) a higher magnification of well-preserved Fmoc-FFpY self-assembled fibers.

Immersing the fluorescent multilayer film in Fmoc-FFpY solution, in the presence of ThT leads to an increase of thickness from 10 to 20 µm (Fig. S4 and Fig. 5a). The red intensity, due to PAH^{rho}, is distributed throughout the cross-section, and the green fluorescence, due to ThT probing the peptide self-assembly, is localized to the upper part (Fig. 5b). The bottom ~4 µm of

the film appears devoid of peptides (Fig. 5c). The top view of the peptide self-assembled on the multilayer film shows fibers distributed around the surface with overlapping of the red fluorescence of PAH^{rho} and the green fluorescence of self-assembled Fmoc-FFpY (Fig. 5d-f). A control experiment confirmed the multilayer film immersed in a solution of ThT presents no green fluorescence in the absence of peptide (Fig. S4). The structure of the self-assembled peptide, observed in cross-section by Cryo-SEM, shows two distinct zones (Fig. 5g). The first zone, adjacent to the silicon substrate, has a thickness of 3.6 µm which corresponds to the PGA/PAH multilayer. Before contact with Fmoc-FFpY, $(PGA/PAH)_{23}$-PGA film appears compact with a thickness around 7 µm (Fig. S5), close to the one observed by CLSM. The second zone, on the top, with a thickness of 23.5 µm, corresponds to the self-assembled peptide, in agreement with the observations made by CLSM. Large cavities on the upper part of the sample are attributed to experimental artifacts due to the formation of ice crystals during cooling followed by their sublimation. A zoom-in of the peptide self-assembly area shows micrometer-long fibers oriented perpendicularly to the interface of the multilayer films, some of which have a helical structure (Fig. 5h and Fig. S6). Similar to coacervates, peptide self-assembly takes place on the surface of the multilayer film with an overlap of PAH chains and Fmoc-FFpY self-assembly.

3.4 Mechanism of the Fmoc-FFpY self-assembly on PGA/PAH Layer-by-Layer film

Peptide self-assembly was monitored *in situ* on PGA/PAH multilayers to verify the role of the PAH diffusion in the mechanism. The entire course of buildup of a $(PGA/PAH)_5$-PGA film , then peptide self-assembly on this film, was followed *in situ* by Quartz Crystal Microbalance (QCM-D) and by ATR-FTIR, which have penetration depths of around 200 nm (resonance frequency at 15 MHz) and 1.5 µm, respectively. After buildup, PGA/PAH film was immersed in

Fmoc-FFpY solution, leading to an increase of the normalized frequency shift up to 45 Hz due to mass uptake (Fig. S7). To prevent PAH diffusion, the multilayer film was cross-linked using carbodiimide chemistry [28] and immersed in the Fmoc-FFpY solution. No frequency shift was observed on injection of the peptide solution (Fig. S8), supporting the requirement for PAH diffusion from the bulk of the film to the Fmoc-FFpY in solution to induce peptide self-assembly. To gain more insight on the self-assembly mechanism, Fmoc-FFpY self-assembly was also followed on PGA/PAH film by ATR-FTIR in deuterated water (Fig. 6).

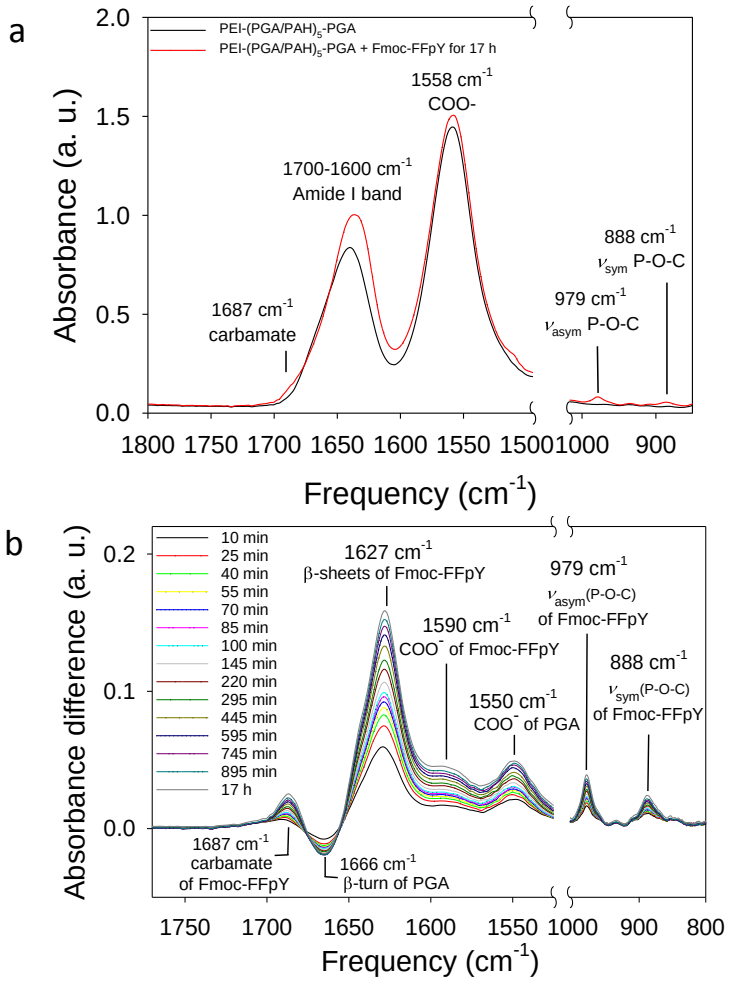

Fig. 6. (a) FTIR spectra of PEI-(PGA/PAH)$_5$-PGA film before and after contact with the Fmoc-FFpY solution for 17 h. (b) Evolution of FTIR difference spectra of PGA/PAH film before and after contact with the Fmoc-FFpY solution as a function of time.

The PGA/PAH film displays an amide I band centered at 1640 cm^{-1} related to PGA (Fig. 6a). After exposure to Fmoc-FFpY solution for 17 h, the amide I band increased in intensity with a slight shift to 1636 cm^{-1} with the appearance of a carbamate shoulder at 1687 cm^{-1} attributed to the peptide. In the same time, the intensity of the carboxylic peak at 1558 cm^{-1} increased and phosphate peaks appeared at 979 and 888 cm^{-1} [29, 30] confirming the phosphorylated form of the peptide (Fig. 6a). The kinetics of the peptide self-assembly can be followed by subtracting the contribution of PGA/PAH film from the spectra (Fig. 6b). An increase of all peptide peaks intensities is observed as a function of time, such as the peaks related to the carbamate (1687 cm^{-1}) [31], the terminal carboxylic acid (1590 cm^{-1}) [32] and phosphate (979 and 888 cm^{-1}) [29] moieties. The increase of β-sheet structure of the amide I band (1627 cm^{-1}), attributed also to the peptide, supports Fmoc-FFpY self-assembly [24, 33]. Regarding PGA peaks, an increase of the carboxylic group (1550 cm^{-1}) and a decrease of β-turn peaks (1666 cm^{-1}) during the peptide self-assembly [34-36] can be observed. The mechanism underlying the peptide self-assembly can be explored by plotting the normalized absorbance intensities of the different peaks as a function of time. A similar evolution of β-sheets (1627 cm^{-1}) and the phosphate (979 cm^{-1}) peaks of the peptide is observed demonstrating that all Fmoc-FFpY peptide self-assembles (Fig. 7a). Concomitantly, the intensity of the PGA carboxylic group peak increases in a similar manner to the β-sheets peak of the peptide (Fig. 7b). This increase is related to carboxylic group dissociation of PGA groups inside the film, as it surrenders PAH groups to phosphates in Fmoc-FFpY. This is supported by the decrease of the β-turn PGA peak at 1666 cm^{-1} during the peptide self-assembly (Fig. 7b). Indeed, PGA solution exhibits a lower β-turn content (18% *vs* 34%) than a mixed solution of PGA and PAH (1:2 PGA/PAH monomer molar ratio) (Fig. S9, Table S1).

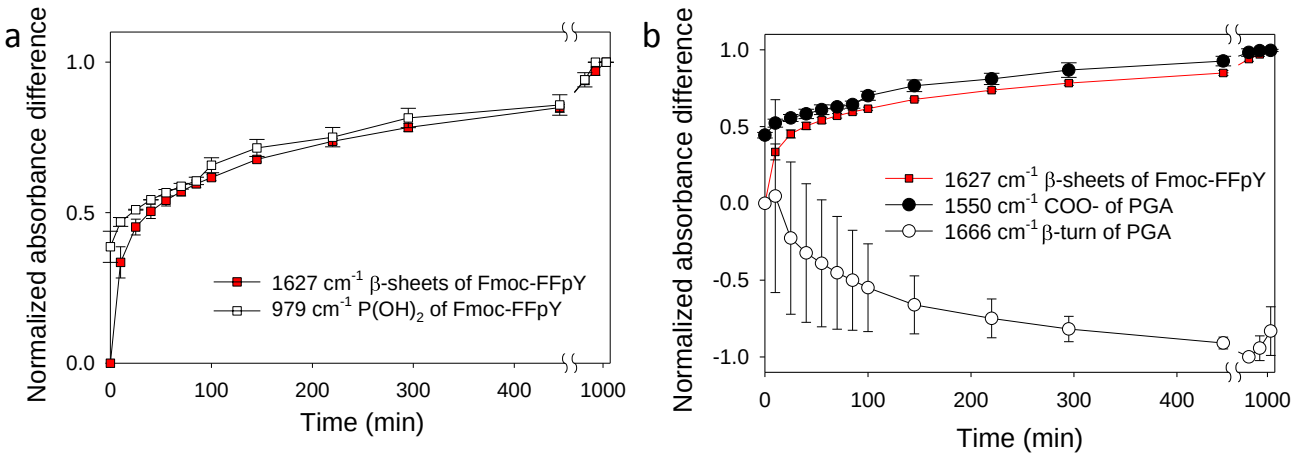

Fig. 7. Evolution of the normalized FTIR absorbance difference intensities as function of the contact time of β-sheets of the peptide in comparison with (a) phosphate peak of the peptide and (b) carboxylic group and β-turn peaks of PGA. The data represent the mean and standard deviation obtained from two independent experiments.

PGA chains, complexed with PAH chains, exchange with the phosphorylated peptides, thanks to a higher association constant of ammonium groups with phosphate groups than with carboxylate groups [37]. The negative charges of PGA must be compensated by counterions from the medium. At the film/solution interface, PAH chains, partially complexed by the phosphorylated peptides, diffuse towards the solution to self-assemble with more Fmoc-FFpY peptides leading to their fibrillar structure. This interaction occurs only when PAH chains are free to diffuse from the film, giving rise to a micrometer thick coating. Because coacervates and polyelectrolyte multilayers have essentially the same composition, a similar mechanism must take place when coacervates enter in contact with the Fmoc-FFpY solution.

4. Conclusions

Based on our previous work showing that Fmoc-FFpY self-assembly can be initiated by ion pairing between the phosphate groups of the peptide and the amine groups of a polycation (PAH) [18], we have demonstrated the localized self-assembly of Fmoc-FFpY on the surface of PGA/PAH complex coacervate microdroplets and multilayers. When PGA/PAH droplets or polyelectrolyte multilayers are immersed in a Fmoc-FFpY solution, the phosphorylated peptide attracts PAH partially out of the PGA/PAH complex and interacts with the PAH chains mainly at the complex/solution interface leading to the formation of self-assembled fibers. The process underlying the attraction of PAH by Fmoc-FFpY is similar to that responsible for the exponential growth of exponentially growing polyelectrolyte multilayers [38] which thus appears rather universal. A next step will consist of using the ability of complex coacervates to partition enzymes [39], to trigger self-assembly processes of peptides not only through electrostatic interactions but also by enzyme-assisted processes localized at or in the coacervates. This would constitute the first totally synthetic mimic of mitotic spindle formation and would represent an important tool to develop synthetic cells.

CRediT authorship contribution statement

Miryam Criado-Gonzalez: Conceptualization, Methodology, Investigation, Formal Analysis, Data curation, Writing - review & editing. **Deborah Wagner**: Methodology, Investigation. **Muhammad Haseeb Iqbal**: Investigation. **Aymeric Ontani**: Investigation. **Alain Carvalho**: Investigation. **Marc Schmutz**: Investigation. **Joseph B. Schlenoff**: Conceptualization, Writing - review & editing. **Pierre Schaaf**: Conceptualization, Supervision, Writing - review & editing,

Funding acquisition, **Loïc Jierry**: Supervision, **Fouzia Boulmedais**: Conceptualization, Data curation, Supervision, Writing - review & editing, Project administration.

Declaration of Competing Interest

The authors declare that they have no known competing financial interests or personal relationships that could have appeared to influence the work reported in this paper.

Acknowledgments

M.H.I. thanks the Higher Education Commission (HEC) Pakistan for his Ph.D. scholarship. J.B.S. thanks the France-USA Fulbright commission. ICS microscopy and ICS characterization platforms are acknowledged for the use of their respective instruments. We gratefully acknowledge financial support from Agence Nationale de la Recherche (EASA, ANR-18-CE06-0025-03) and Institut Carnot MICA (DIAART).

References

[1] V.N. Uversky, Intrinsically disordered proteins in overcrowded milieu: Membrane-less organelles, phase separation, and intrinsic disorder, Curr. Opin. Struct. Biol. 44 (2017) 18-30.

[2] P.T. Conduit, A. Wainman, J.W. Raff, Centrosome function and assembly in animal cells, Nat. Rev. Mol. Cell Biol. 16(10) (2015) 611-624.

[3] J.A. Toretsky, P.E. Wright, Assemblages: Functional units formed by cellular phase separation, J. Cell Biol. 206(5) (2014) 579-588.

[4] C.D. Keating, Aqueous Phase Separation as a Possible Route to Compartmentalization of Biological Molecules, Acc. Chem. Res. 45(12) (2012) 2114-2124.

[5] G.A. Mountain, C.D. Keating, Formation of Multiphase Complex Coacervates and Partitioning of Biomolecules within them, Biomacromolecules 21(2) (2020) 630-640.

[6] B.C. Buddingh, J.C.M. van Hest, Artificial Cells: Synthetic Compartments with Life-like Functionality and Adaptivity, Acc. Chem. Res. 50(4) (2017) 769-777.

[7] C.M. Agapakis, P.M. Boyle, P.A. Silver, Natural strategies for the spatial optimization of metabolism in synthetic biology, Nat. Chem. Biol. 8(6) (2012) 527-535.

[8] A.H. Chen, P.A. Silver, Designing biological compartmentalization, Trends Cell Biol. 22(12) (2012) 662-670.

[9] B. Stadler, R. Chandrawati, A.D. Price, S.F. Chong, K. Breheney, A. Postma, L.A. Connal, A.N. Zelikin, F. Caruso, A Microreactor with Thousands of Subcompartments: Enzyme-Loaded Liposomes within Polymer Capsules, Angew. Chem. Int. Ed. 48(24) (2009) 4359-4362.

[10] R.J.R.W. Peters, M. Marguet, S. Marais, M.W. Fraaije, J.C.M. van Hest, S. Lecommandoux, Cascade Reactions in Multicompartmentalized Polymersomes, Angew. Chem. Int. Ed. 53(1) (2014) 146-150.

[11] R.J.R.W. Peters, I. Louzao, J.C.M. van Hest, From polymeric nanoreactors to artificial organelles, Chem. Sci. 3(2) (2012) 335-342.

[12] H.-C. Chiu, Y.-W. Lin, Y.-F. Huang, C.-K. Chuang, C.-S. Chern, Polymer Vesicles Containing Small Vesicles within Interior Aqueous Compartments and pH-Responsive Transmembrane Channels, Angew. Chem. Int. Ed. 47(10) (2008) 1875-1878.

[13] S.F.M. van Dongen, W.P.R. Verdurmen, R.J.R.W. Peters, R.J.M. Nolte, R. Brock, J.C.M. van Hest, Cellular Integration of an Enzyme-Loaded Polymersome Nanoreactor, Angew. Chem. Int. Ed. 49(40) (2010) 7213-7216.

[14] A.F. Mason, N.A. Yewdall, P.L.W. Welzen, J. Shao, M. van Stevendaal, J.C.M. van Hest, D.S. Williams, L.K.E.A. Abdelmohsen, Mimicking Cellular Compartmentalization in a Hierarchical Protocell through Spontaneous Spatial Organization, ACS Cent. Sci. 5(8) (2019) 1360-1365.

[15] P.M. McCall, S. Srivastava, S.L. Perry, D.R. Kovar, M.L. Gardel, M.V. Tirrell, Partitioning and Enhanced Self-Assembly of Actin in Polypeptide Coacervates, Biophys. J. 114(7) (2018) 1636-1645.

[16] C. Vigier-Carriere, T. Garnier, D. Wagner, P. Lavalle, M. Rabineau, J. Hemmerle, B. Senger, P. Schaaf, F. Boulmedais, L. Jierry, Bioactive Seed Layer for Surface-Confined Self-Assembly of Peptides, Angew. Chem. Int. Ed. 54(35) (2015) 10198-10201.

[17] M. Criado-Gonzalez, J.R. Fores, A. Carvalho, C. Blanck, M. Schmutz, L. Kocgozlu, P. Schaaf, L. Jierry, F. Boulmedais, Phase Separation in Supramolecular Hydrogels Based on Peptide Self-Assembly from Enzyme-Coated Nanoparticles, Langmuir 35(33) (2019) 10838-10845.

[18] M. Criado-Gonzalez, D. Wagner, J. Rodon Fores, C. Blanck, M. Schmutz, A. Chaumont, M. Rabineau, J.B. Schlenoff, G. Fleith, J. Combet, P. Schaaf, L. Jierry, F. Boulmedais, Supramolecular Hydrogel Induced by Electrostatic Interactions between Polycation and Phosphorylated-Fmoc-Tripeptide, Chem. Mater. 32(5) (2020) 1946-1956.

[19] K.A. Black, D. Priftis, S.L. Perry, J. Yip, W.Y. Byun, M. Tirrell, Protein Encapsulation via Polypeptide Complex Coacervation, ACS Macro Letters 3(10) (2014) 1088-1091.

[20] A.B. Marciel, S. Srivastava, M.V. Tirrell, Structure and rheology of polyelectrolyte complex coacervates, Soft Matter 14(13) (2018) 2454-2464.

[21] W. Ji, C. Yuan, S. Zilberzwige-Tal, R. Xing, P. Chakraborty, K. Tao, S. Gilead, X. Yan, E. Gazit, Metal-Ion Modulated Structural Transformation of Amyloid-Like Dipeptide Supramolecular Self-Assembly, ACS Nano 13(6) (2019) 7300-7309.

[22] M.J. Krysmann, V. Castelletto, A. Kelarakis, I.W. Hamley, R.A. Hule, D.J. Pochan, Self-assembly and hydrogelation of an amyloid peptide fragment, Biochemistry 47(16) (2008) 4597-4605.

[23] C. Tang, R.V. Ulijn, A. Saiani, Effect of Glycine Substitution on Fmoc–Diphenylalanine Self-Assembly and Gelation Properties, Langmuir 27(23) (2011) 14438-14449.

[24] A.M. Smith, R.J. Williams, C. Tang, P. Coppo, R.F. Collins, M.L. Turner, A. Saiani, R.V. Ulijn, Fmoc-Diphenylalanine Self Assembles to a Hydrogel via a Novel Architecture Based on π–π Interlocked β-Sheets, Adv. Mater. 20(1) (2008) 37-41.

[25] T.J. Halthur, U.M. Elofsson, Multilayers of Charged Polypeptides As Studied by in Situ Ellipsometry and Quartz Crystal Microbalance with Dissipation, Langmuir 20(5) (2004) 1739-1745.

[26] L. Jourdainne, S. Lecuyer, Y. Arntz, C. Picart, P. Schaaf, B. Senger, J.-C. Voegel, P. Lavalle, T. Charitat, Dynamics of Poly(l-lysine) in Hyaluronic Acid/Poly(l-lysine) Multilayer Films Studied by Fluorescence Recovery after Pattern Photobleaching, Langmuir 24(15) (2008) 7842-7847.

[27] F. Boulmedais, V. Ball, P. Schwinte, B. Frisch, P. Schaaf, J.-C. Voegel, Buildup of Exponentially Growing Multilayer Polypeptide Films with Internal Secondary Structure, Langmuir 19(2) (2003) 440-445.

[28] R. Zahn, G. Coullerez, J. Vörös, T. Zambelli, Effect of polyelectrolyte interdiffusion on electron transport in redox-active polyelectrolyte multilayers, J. Mater. Chem. 22(22) (2012) 11073-11078.

[29] B.J.M. Rajkumar, V. Ramakrishnan, Vibrational spectroscopic study of dl-methionine dihydrogen phosphate, Spectrochim. Acta A Mol. Biomol. Spectrosc. 57(2) (2001) 247-254.

[30] R.A. Nyquist, Interpreting Infrared, Raman, and Nuclear Magnetic Resonance Spectra, Academic Press, San Diego, 2001.

[31] S. Fleming, P.W.J.M. Frederix, I.R. Sasselli, N.T. Hunt, R.V. Ulijn, T. Tuttle, Assessing the Utility of Infrared Spectroscopy as a Structural Diagnostic Tool for beta-Sheets in Self-Assembling Aromatic Peptide Amphiphiles, Langmuir 29(30) (2013) 9510-9515.

[32] C. Tang, A.M. Smith, R.F. Collins, R.V. Ulijn, A. Saiani, Fmoc-Diphenylalanine Self-Assembly Mechanism Induces Apparent pKa Shifts, Langmuir 25(16) (2009) 9447-9453.

[33] J. Kong, S. Yu, Fourier Transform Infrared Spectroscopic Analysis of Protein Secondary Structures, Acta Biochim. Biophys. Sin. 39(8) (2007) 549-559.

[34] H. Lenormant, A. Baudras, E.R. Blout, Reversible Configurational Changes in Sodium Poly-α,L-glutamate Induced by Water1, J. Am. Chem. Soc. 80(23) (1958) 6191-6195.

[35] J.L. Koenig, B. Frushour, Raman studies of the helix-to-coil transition in poly-L-glutamic acid and poly-L-ornithine, Biopolymers 11(9) (1972) 1871-1892.

[36] M. Jackson, P.I. Haris, D. Chapman, Conformational transitions in poly(l-lysine): studies using Fourier transform infrared spectroscopy, Biochim. Biophys. Acta Protein Struct. Mol. Enzymol. 998(1) (1989) 75-79.

[37] B. Springs, P. Haake, Equilibrium constants for association of guanidinium and ammonium ions with oxyanions: The effect of changing basicity of the oxyanion, Bioorg. Chem. 6(2) (1977) 181-190.

[38] P. Lavalle, C. Picart, J. Mutterer, C. Gergely, H. Reiss, J.-C. Voegel, B. Senger, P. Schaaf, Modeling the buildup of polyelectrolyte multilayer films having exponential growth, J. Phys. Chem. B 108(2) (2004) 635-648.

[39] W.M. Aumiller, C.D. Keating, Experimental models for dynamic compartmentalization of biomolecules in liquid organelles: Reversible formation and partitioning in aqueous biphasic systems, Adv. Colloid Interface Sci. 239 (2017) 75-87.